Available online at www.sciencedirect.com

ScienceDirect

journal homepage: www.intl.elsevierhealth.com/journals/dema

Miniature specimens for fracture toughness evaluation of dental resin composites

Herzl Chai[a,*], *Xiaohong Wang*[b], *Jirun Sun*[b,**]

[a] *School of Mechanical Engineering, Tel Aviv University, Tel Aviv 6997801, Israel*
[b] *Anthony Volpe Research Center, American Dental Association Foundation, Gaithersburg, MD 20899, USA*

ARTICLE INFO

Article history:
Received 24 August 2018
Received in revised form
8 November 2018
Accepted 15 November 2018

Keywords:
Miniature specimens
Fracture toughness
Edge chipping
Dental resin composites
Resin chemistry

ABSTRACT

Objective. Millimeter-scale ("miniature") specimens enable *in-situ* evaluation of mechanical properties of engineering materials at reduced cost. Here three such specimens for measuring fracture toughness (K_C) are developed and implemented to new dental materials. The latter include concurrent methacrylate-based and new ether-based resin composites designed to reduce polymerization stress and enhance service life in restored teeth.

Methods. Fracture toughness of four experimental and one commercial dental resin composites are evaluated using three-point bending (3PB), wedge double-cantilever-beam (WDCD) and edge chipping miniature test specimens. The values of K_C were compared with those obtained following ISO standard method ISO6872: 2014. The stress intensity factor (K) for the 3PB and WDCB specimens was determined using linear fracture mechanics analyses made in conjunction with the Finite Element technique, with due consideration given to the finite width of pre-crack.

Results. Analytic expressions for predicting K_C were developed for all three miniature specimens. The width of pre-crack, generally neglected for conventional specimens, significantly affect K. Measured K_C conclusively agree with those of commercial or well-studied materials as obtained using conventional specimens, with error bounded by 5–10 percent.

Significance. The edge chipping test was successfully applied for the first time to non-brittle materials like dental resin composites. The miniature specimens developed will expedite the evaluation of fracture toughness of dental resin composites by saving materials and provide needed *in-situ* assessment capability. The chipping test which requires no introduction of initial crack and involves no use of elastic constants is especially suitable to functionally graded materials and *in-situ* study of restored teeth. The WDCB specimen enables stable crack growth, a useful trait in fatigue studies.

1. Introduction

Fracture toughness (K_C) is a primary quantity in assessing fracture resistance of dental resin composites used for cavity filling in restored teeth. This quantity has been evaluated using numerous test specimens including compact tension, Chevron notched rod, double-torsion and notched three-point bending specimens. Fujishima and Ferracane conducted a comparative study of these specimens using two experimen-

* *Corresponding author.*
** *Corresponding author at*: 100 Bureau Drive, Stop 8546, Gaithersburg, MD 20899-8546, USA.
E-mail addresses: herzl@eng.tau.ac.il (H. Chai), jsun@nist.gov (J. Sun).

https://doi.org/10.1016/j.dental.2018.11.023
0109-5641/

Fig. 1 – Failure of human molar tooth restored with dental resin composite due to indentation by 6.3 mm diameter tungsten/carbide (W/C) ball laid at the central fossa [9]. Chipping in the composite immediately followed debonding between composite and tooth structure.

tal and three commercial dental composites [1]. The resulting K_C varied significantly among the specimens, and furthermore it was affected by crack tip sharpness. The effect of filler compositions, whether in homogeneous or hybrid micro/nano particle filler forms, has been systematically established [2–4]. Large data scatter notwithstanding, K_C generally increase with filler's volume fraction before stabilizing at about 60% (or 80% by filler weight). Other studies dealt with more particular aspects of material toughness including aging, cyclic loading and degree of conversion (DC) of the resin constituent [3,5].

Dental resin composites are gaining popularity for treating dental caries due to their aesthetics, strong adhesion to teeth and clinical readiness for small/large and anterior/posterior restorations [6,7]. However, the average service life of these materials is generally limited by frequent fracturing and development of secondary caries [8]. An example of the type of failure encountered in the applications of current dental composites is shown in Fig. 1. The specimen shown corresponds to a human molar tooth subjected to mesial-occlusal-distal restoration [9]. Following indentation by a hard ball freely laid at the central fossa, the tooth failed by edge chipping. The latter occurred immediately after the debonding of filling from tooth structure. To overcome such problems, new dental resin composites are being developed using hydrolytically stable resin network [10–14], self-healing technology [15–17] and antimicrobial additives [18–21]. Resistance to crack propagation over time is vital for making durable restoration in oral environments. For this purpose, techniques for a proper evaluation of K_C using minimal amount of material are needed.

This work is aimed at developing small-size specimens for determining K_C at reduced cost and under *in-situ* environment and implementing the results to new dental resin composites. Use of such specimens pose experimental and analytical challenges including accounting for the effect of crack-tip plastic deformation and finite thickness of pre-crack. The approach used includes testing and fracture mechanics analyses in conjunction of the Finite Element (FE) technique.

2. Materials and methods

2.1. *Materials*

The methacrylate monomers, urethane dimethacrylate (UDMA), triethylene glycol dimethacrylate (TEGDMA) and a mixture of bisphenol A glycidyl dimethacrylate (Bis-GMA)/TEGDMA used in this study were obtained from Esstech Inc. (Essington, PA, USA). The ether-based monomer, triethylene glycol-divinylbenzyl ether (TEG-DVBE), was synthesized and fully characterized in our laboratory as reported in [10]. All monomer mixtures were activated for photo-polymerization by adding 0.2 wt % of photo-oxidant, camphorquinone (CQ; Aldrich, Saint Louis, MO, USA) and 0.8 wt % of photo-reductant, ethyl 4-*N*,*N*-dimethylaminobenzoate (4EDMAB; Aldrich, Saint Louis, MO, USA).

2.1.1. *Composites fabrication*

Each composite contained 25 wt % (mass fraction) resin, 67.5 wt % silanized $BaBFAlSiO_4$ milled glass (Product code #907643, Dentsply, York, PA, USA) and 7.5 wt % AEROSIL® OX 50 nanoparticles (Evonik Industries, Essen, Germany). These components were mixed by a speed mixer (DAC 150 FVZ, Flack-Tek, Landrum, SC, USA) at 3500 rpm for 1 min, and then hand mixed for additional 1 min. The mixing process was repeated 3 times to obtain a uniform clay-like paste.

A Bis-GMA-based commercial composite, Filtek Z250 (A1 shade, 3 M ESPE, St. Paul, MN, USA) was also used as a reference dental resin composite. This material has 82 wt % filler with 0.01–3.5 μm particles. Table 1 lists the monomer compositions of the five composites used in this study, henceforth labeled as materials 0–4.

Ten orthogonal blocks of dimensions (25 mm × 3 mm × 4 mm) were prepared for each one of the 5 dental composites. Samples were prepared by inserting composite paste into 25 mm × 3 mm × 4 mm stainless-steel mold which surfaces covered by Mylar films. The specimen bars were cured (2 min/each open side of the mold) using a Dentsply Triad 2000 visible light curing unit (Dentsply, York, PA, USA) with a tungsten halogen light bulb (75 W and 120 V, 43 mW/cm^2). Test specimens were prepared from these material blocks as described below.

2.1.2. *Degree of conversion (DC)*

The DC was evaluated 24 h after curing using a Thermo Nicolet Nexus 670 FT-IR spectrometer (Thermo Scientific, Madison, Wisconsin, USA) with a KBr beam splitter, an MCT/A detector and an attenuated total reflectance (ATR) accessory. The aromatic C=C absorption band at 1608 cm^{-1} of Bis-GMA and the amide group band of UDMA at 1537 cm^{-1} were used as the internal standards for materials 0 & 2 and materials 1, 3 & 4, respectively. The areas of absorption peaks of the vinyl group of TEG-DVBE at 1629 cm^{-1} and the methacrylate groups

Table 1 – Composition of resin monomers in the dental resin composites.

Material	DC (%)	Resin (wt%)			
		UDMA	TEG-DVBE	Bis-GMA	TEGDMA
0	62.0(1.0)	Z250-Commercial Bis-GMA/TEGDMA based material			
1	79.2(1.9)	55.8	44.2	–	–
2	62.0(2.6)	–	–	69.3	29.7
3	80.2(3.1)	61.6	–	–	31.4
4	70.3(1.2)	78.3	20.7	–	–

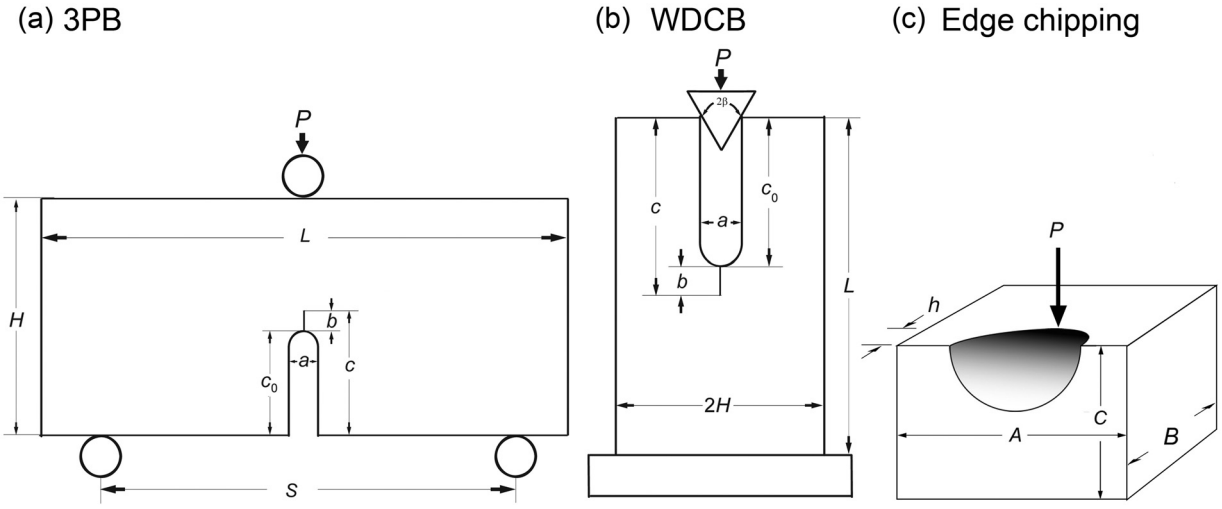

Fig. 2 – The 3PB (a), WDCB (b) and edge chipping (c) specimens used for evaluating fracture toughness K_C of dental resin composites. Initial cracks of width a and length c_0 were introduced in (a) and (b) by a diamond-coated disk. The force P in (b) is applied by W/C wedge of total angle $2\beta = 60°$. The load in (c) is applied by a Vickers pyramid which edges aligned normal/parallel to a free surface. To reduce friction, a double-layer Teflon tape was inserted between all moving parts.

of UDMA, TEGDMA or Bis-GMA at 1638 cm^{-1} were integrated. Peaks were resolved by employing the curve fitting program Fityk (version 0.9.8). The degree of conversion was calculated from DC (%) = 100[$(A_1/A_0 - A_1'/A_0')/(A_1/A_0)$], where A_1/A_0 and A_1'/A_0' represent the peak-area-ratio of vinyl (both monomers in each system) and internal standard before and after polymerization, respectively [22,23].

2.2. *Test specimens*

As shown in Fig. 2 three specimens were used to evaluate fracture toughness K_C: three-point bending (3PB) (a), wedge double-cantilever-beam (WDCB) (b) and edge chipping (c). The first is commonly used for dental composites due to its simplicity. The WDCB specimen, while more involved, is especially useful for evaluating fracture toughness in non-homogeneous systems such as dental adhesives bonded to ceramics substrates [24]. The chipping test, originally used for measuring 'edge toughness' of brittle materials [25–27], was shown to be capable of producing K_C, a material property independent of specimen geometry [28]. Previous uses of this approach were limited to brittle ceramics, however, with reported K_C values generally within several percent of those measured in control tests [28–32]. Here we apply millimeter-scale version of these specimens, referred to as "miniature". To assess the merit of the latter, K_C was also evaluated using a standard 3PB specimen ("control").

2.2.1. *Control specimen*

Reference K_C values were generated using the ISO standard method ISO6872: 2014. As shown in Fig. 2a this 3PB specimen has length, support span, thickness and width (L, S, H, B) of (25, 20, 4, 3) mm, in that order. A pre-crack $c_0 = 1.2$ mm was introduced into the specimens using a diamond-coated disk of thickness $a = 0.33$ mm. A sharp crack $b = 1.0$ mm long was then produced at the base of the cut by a razor blade, resulting in total crack length $c = 2.2$ mm.

All miniature specimens were produced from fractured control specimens. The latter were cut to desired dimensions as specified below using common metallographic procedures.

2.2.2. *Miniature test specimens*

The dimensions of the miniature 3PB specimen (Fig. 2a) were (L, S, H, B) = (12, 10, 2, 3) mm. The width of the saw cut a was 0.13 mm, corresponding to the smallest commercially available rotary disk, while the length of the cut c_0 varied from 0.2 to 0.8 mm. The smallness of a precluded creating a sharp crack using razor blade so that the fracture occurred naturally from the cut terminus. All 3PB specimens were supported by 2 mm radius cylindrical steel rods while loaded at their mid span by force P using a similar rod. The WDCB specimen (Fig. 2b) has dimensions ($2H$, L, B) = (4, 7.5, 3) mm. A pre-crack was introduced at the specimen midplane similarly to the miniature 3PB specimen. The crack length c_0 varied over the range 1.8–3.5 mm. The specimens were clamped by a vice over 2 mm

long span and then loaded at their edge by a wedge. The latter had angle $2\beta = 60^\circ$, which was grounded on a 9.5 mm diameter silicon carbide rod. The edge chipping specimens (Fig. 2c) were of dimensions (A, B, C) = (4, 3, 4) mm. The specimens were laid on x–y micrometer stage and indented a distance h from a free surface by Vickers pyramid which corners aligned normal/parallel to the surface. The indent distance, measured after unloading using optical microscopy, ranged from 0.2 to 1.3 mm.

All test specimens were loaded using a standard loading frame operated at the displacement rate of 0.05 mm/min. To reduce friction, a double layer of thin Teflon strip was placed between all moving parts including supporting pins and wedge. The fracture process was monitored using a video camera (Cannon EOS-5D) equipped with a zoom lens (Optem, Inc.). The applied force and machine displacement were continuously recorded during the tests. The fracture surfaces were examined by optical microscopy.

2.3. *Fracture mechanics analysis*

Calculations of stress intensity factor (SIF) K for 3PB specimens are generally limited to sharp crack $a = 0$, a valid assumption when pre-crack b at the saw cut is sufficiently long. In the case of miniature 3PB and WDCB specimens no sharp pre-crack was introduced. The SIF K in this case was determined with the aid of a commercial FEM code (Ansys Inc., version 14) specified to 2-D plane-stress conditions. With friction coefficient μ of Teflon ≈ 0.04 [33], the effect of friction was conclusively neglected. A sharp crack, length b, was taken to emanate from the semi-circular base of the saw cut, resulting in total crack length $c = c_0 + b$ (Fig. 2a–b). The load transmitted from wedge to arms of the WDCB specimen was broken into vertical and horizontal components P/2 and P/2tanβ, respectively. The SIF K was calculated in accord with Irwin's crack opening displacement approach as detailed in [24]. The Young's modulus E and Poisson's ratio ν of the composites were taken as 11 GPa and 0.35. Up to 8000 four-node isoparametric elements were used in the FEA. The mesh was refined until K converged to within 1–2%. The results of the FEA including choice of initial pre-crack b are discussed in Section 3.1.

The fracture toughness for the edge chipping test was determined from Ref. [28]

$$K_C = P_F/(9.3h^{1.5}) \quad (1)$$

where P_F is the force needed to cause chipping, a distinct event associated with a complete load drop. As was shown in Ref. [31], Eq. (1) is valid only if the force at which median-radial cracks initiate under the contact, P_m, is less than P_F. P_m was shown to depend on tool sharpness and material type; Vickers indentation studies on soda-lime glass and zirconia yielded $P_m \approx 46$ and ≈ 68 N, corresponding to critical indent distance $h_c \approx 0.4$ and ≈ 0.15 mm, respectively [31]. For dental composites both P_m and h_c are expected to be relatively large owing to material plasticity. Accordingly, for the present composites care was taken to insure $h > h_c$.

3. Results

3.1. *Fracture analysis*

3.1.1. 3PB

Fig. 3a (symbols) plots normalized SIF K *vs.* c/H for the miniature 3PB specimen, where

$$\underline{K} \equiv KBH^{1/2}/P \quad (2)$$

Results are given for the three choices $(c_0, a) = (0.23, 0.16)$, (0.6, 0.16), (0.1, 0.08) mm. The solid-line curve in this print corresponds to the case $a = 0$ that represents the "control" specimen [34]:

$$\underline{K}_0 = (16\pi\underline{x})^{1/2}(1.6 - 2.6\underline{x} + 12.3\underline{x}^2 - 21.2\underline{x}^3 + 21.8\underline{x}^4), \underline{x} \equiv c/H \quad (3)$$

The present data seem to approach this curve for sufficiently large c/H. (Note that Eq. (3) corresponds to $S/H = 4$ whereas the present analysis considered $S/H = 5$. This alludes to a small effect of S/H on K, in line with the results in Ref. [35]). The data in Fig. 3a are alternatively presented in Fig. 3b as K/K_0 *vs.* relative local crack length b/a. The data seem to be well fitted by the following solid-line curve

$$f_B \equiv K/K_0 = 1 - \exp[-8.5(b/a)^{0.7}] \quad (4)$$

As evident, when b/a is less than ≈ 0.5 the cut width a need be considered in the fracture analysis.

3.1.2. WDCB

Fig. 4a plots $\underline{K}$ *vs.* c/H for the case of sharp crack ($a = 0$), with symbols representing FEA [24] and solid-line curve an empirical fit:

$$\underline{K}_0 = 19.4[(1 + 0.121\underline{x} + 11.283\underline{x}^2 + 8.698\underline{x}^3)/(1 + 580\underline{x} - 77\underline{x}^2 + 13\underline{x}^3 - 0.8\underline{x}^4)]^{1/2}, \underline{x} \equiv c/H \quad (5)$$

The data exhibit trend reversal at $c/H \approx 0.3$, reflecting a transition from wedge to double-cantilever-beam (DCB) configuration. Fig. 4b plots K/K_0 *vs.* b/a for three choices of crack width a: 0.08, 0.16 and 0.32 mm. As in Fig. 3b, the data tend to fall on the same curve, now represented by

$$f_W \equiv K/K_0 = 1 - \exp[-7(b/a)^{0.7}] \quad (6)$$

The dashed lines in Fig. 4a are the asymptotic limits for wedge [36] and DCB [37] specimens:

$$\text{Wedge}: \underline{K}_0 = (1.2/\tan\beta - \alpha_0)/(\pi c/H)^{1/2}, \alpha_0 \equiv 0.78 \quad (7a)$$

$$\text{DCB}: \underline{K}_0 = 3^{1/2}(c/H)/\tan\beta \quad (7b)$$

The coefficient α_0 in Eq. (7)a represents the effect of compression force P/2 transmitted to each one of the two split arms. For $\beta > 53^\circ$, the SIF becomes negative.

To determine K_C for the 3PB and WDCB specimens, a flaw size $b = c_F$ (Fig. 2) need be specified. The latter was taken to

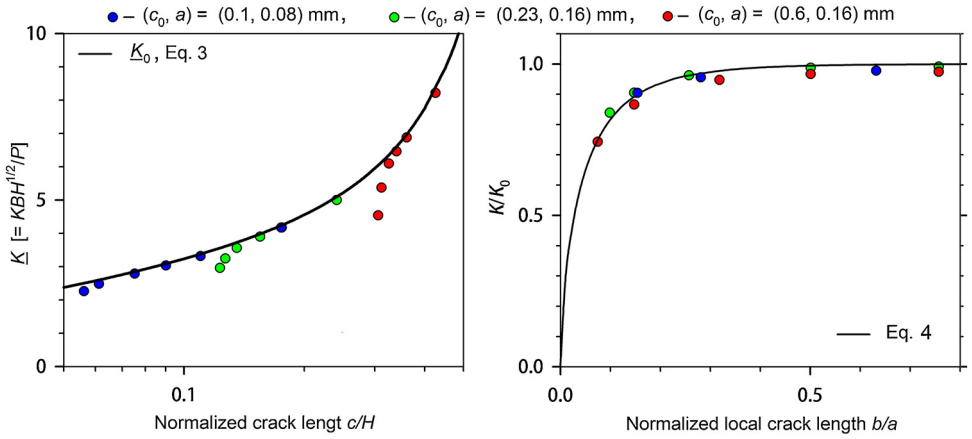

Fig. 3 – FEM results for the miniature 3PB specimen: (a) Normalized SIF $\underline{K}$ *vs.* normalized crack length c/H for three different sets of variables. The solid-line curve represents the case of a sharp crack ($a = 0$, Eq. (3)). (b) Normalized SIF *vs.* relative local crack length b/a for the three cases given in (a). The solid-line curve is an empirical fit (Eq. (4)).

coincide with the intrinsic flaw of the material as found using the edge crack relationship [37].

$$c_F = (K_C/1.12\sigma_F)^2/\pi \quad (8)$$

where σ_F is the composite's failure stress. Using typical values $\sigma_F = 120$ MPa, $K_C = 1.5$ MPa m$^{1/2}$ yields $c_F = 0.04$ mm. This value was conclusively used when calculating K_C. Accordingly, the fracture toughness K_C for the miniature 3PB and WDCB is given by

$$K_C = f\underline{K}_0 P_F/BH^{1/2}, b = c_F \quad (9)$$

where P_F is the fracture force and $\underline{K}_0$ and f are given in Eqs. (3) and (4) (3PB) or Eqs. (5) and (6) (WDCB).

3.2. *Experimental results*

Fig. 5 shows typical fracture surfaces for 3PB (a), WDCB (b) and edge chipping (c) specimens. The cracks in Fig. 5a–b extend collinearly from the saw cut. The chip morphology (c) resembles those found for brittle materials albeit with somewhat larger permanent deformation under the contact. The latter is too small compared with the size of chipping crack or indent distance h to affect the calculation of K_C. The fracture conclusively occurred by a rapid load drop. For edge chipping, K_C was found from Eq. (1) with indent distance h determined as shown in Fig. 5c. For the 3PB and WDCB specimens K_C was determined from Eq. (9) using corresponding values of fracture force P_F and crack length c ($= c_0 + c_F$).

Fig. 6 plots the test results. Fig. 6a–b depict K_C *vs.* normalized initial crack length c_0/H for the miniature 3PB (a) and WDCB (b) specimens, with material choices as specified. Notwithstanding scatter, the data seem insensitive to crack length. Fig. 6c plots K_C *vs.* indent distance h from the edge chipping test. As shown in the left-side print, for given material the data generally exhibit large scatter for relatively small h while tending to level off toward a specific value as h becomes sufficiently large. The transition between these two regimes occurs at $h \approx 0.57$ mm. As discussed in Section 2.3, the first

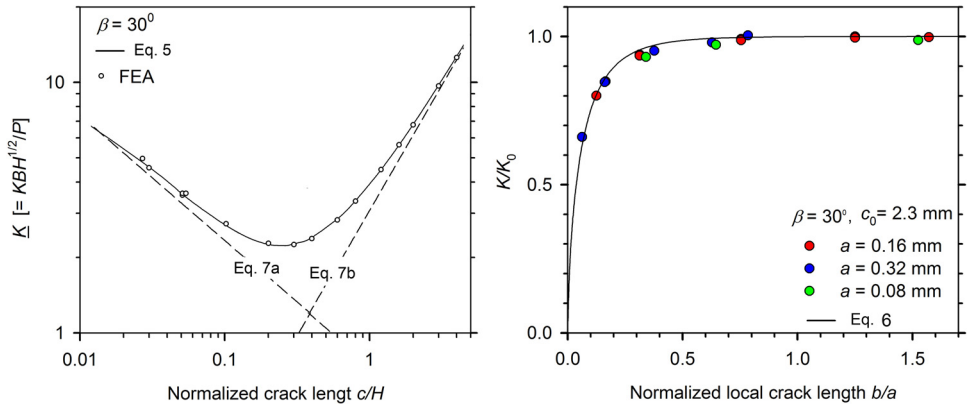

Fig. 4 – FEM results for the miniature WDCB specimen. (a) Normalized SIF $\underline{K}$ *vs.* normalized crack length c/H for sharp crack $a = 0$ and wedge angle $2\beta = 60°$. The data exhibit trend reversal at $c/H \approx 0.3$, reflecting transition from wedge to DCB specimen configurations. The solid line is an empirical fit (Eq. (5)) while the dashed lines are asymptotes for wedge (Eq. (7)a) and DCB (Eq. (7)b). (b) Normalized SIF *vs.* relative local crack length b/a for three choices of cut width a. The solid-line curve is an empirical fit (Eq. (6)).

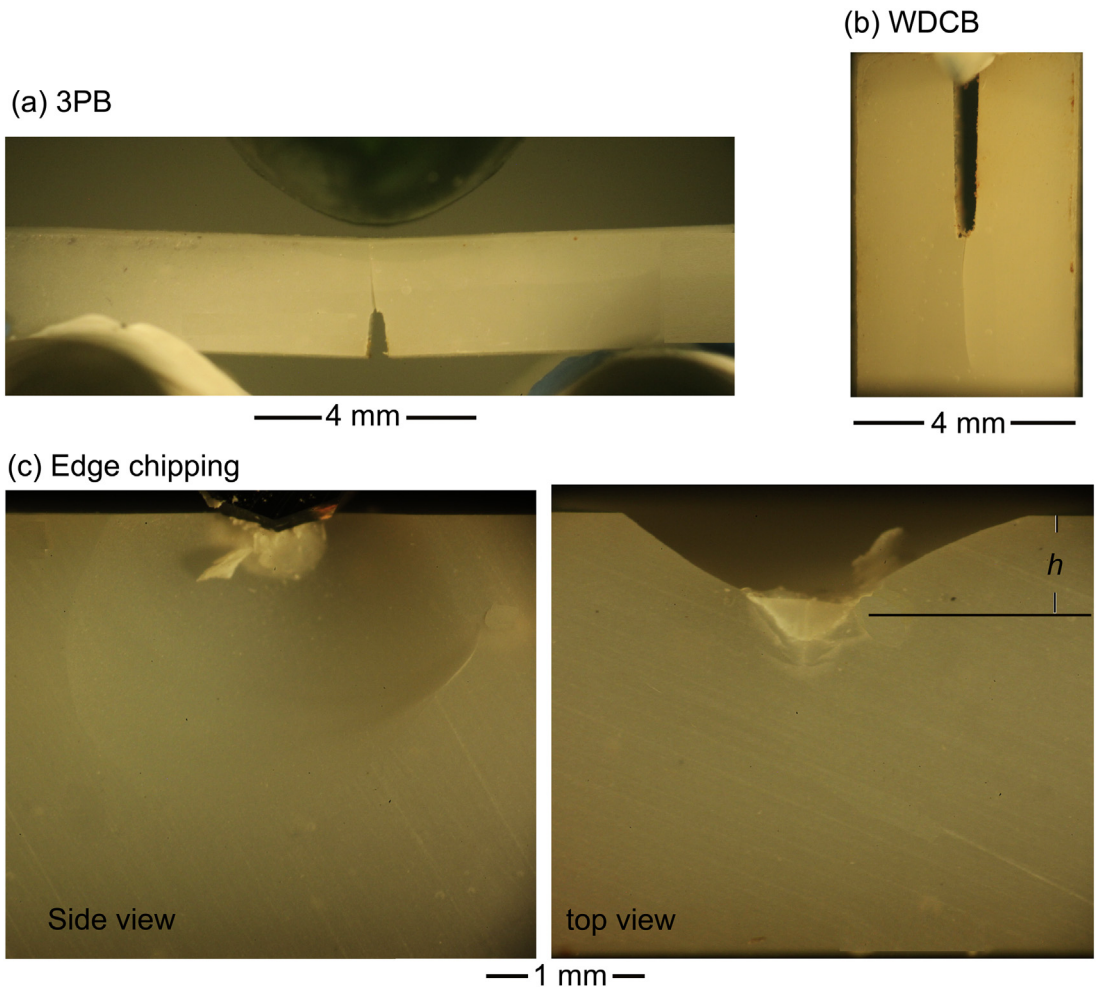

Fig. 5 – Typical post-mortem video images for the 3PB, material 3 (a), WDCB, material 3 (b) and edge chipping, material 2 (c) specimens; the left and right-side frames in (c) correspond to side and top views, respectively.

regime is deemed invalid because the chipping likely followed immediately the onset of median cracks under the indenter. The right-side print in Fig. 6c shows the valid range of K_C. The mean K_C values are shown as horizontal lines in Fig. 6a–c.

Fig. 7 and Table 2 summarize the K_C data (mean and standard deviation (SD)) generated by all control and miniature specimens tested. As shown, the mean K_C from the three miniature specimens is within 1–10% of the control. The notable reduction in K_C for material 2 as compared to all other materials may be attributed to the use of Bis-GMA/TEGDMA resin and low DC.

4. Discussion

Miniature 3PB, wedge and edge chipping specimens were developed to evaluate fracture toughness K_C. Tests were conducted on current and experimental dental resin composites designed to reduce shrinkage after cure. Frictional effects were practically eliminated by placing thin Teflon strips between all moving parts. (It is interesting to note that some preliminary tests on WDCB specimens employing no Teflon strips between loading wedge and split arms yielded ≈20% larger apparent K_C). The calculated K_C was generally within 1–10% of control values (Fig. 7). The relatively large error in miniature specimens is believed to be due mostly to loading misalignments and errors in measuring specimen dimensions that invariably tend to increase with reducing specimen dimensions. For example, in edge chipping a change of indent distance h from 0.6 to 0.7 mm entails 26% increase in K_C. Accordingly, the miniature specimens are useful for determining K_C to within 10% error. (Our specimens were photo-cured from both sides using a long curing depth (>3 mm) photo-initiator. Previous studies showed the same DC at the top and bottom surfaces from light irradiation for specimen thickness smaller than 3 mm [38]. Hence, no powdered samples are necessary for DC determination).

Each one of the miniature specimens studied has its own merit and drawbacks. Unlike for some popular indentation tests, the edge chipping test requires no introduction of pre-crack or use of elastic constants and material hardness in calculating K_C. Moreover, the effect of plastic deformation under the contact is negligible given that the size of this deformation is small compared to that of the chipping crack or indent distance h. On the other hand, care must be taken to ensure that h is sufficiently large so that median

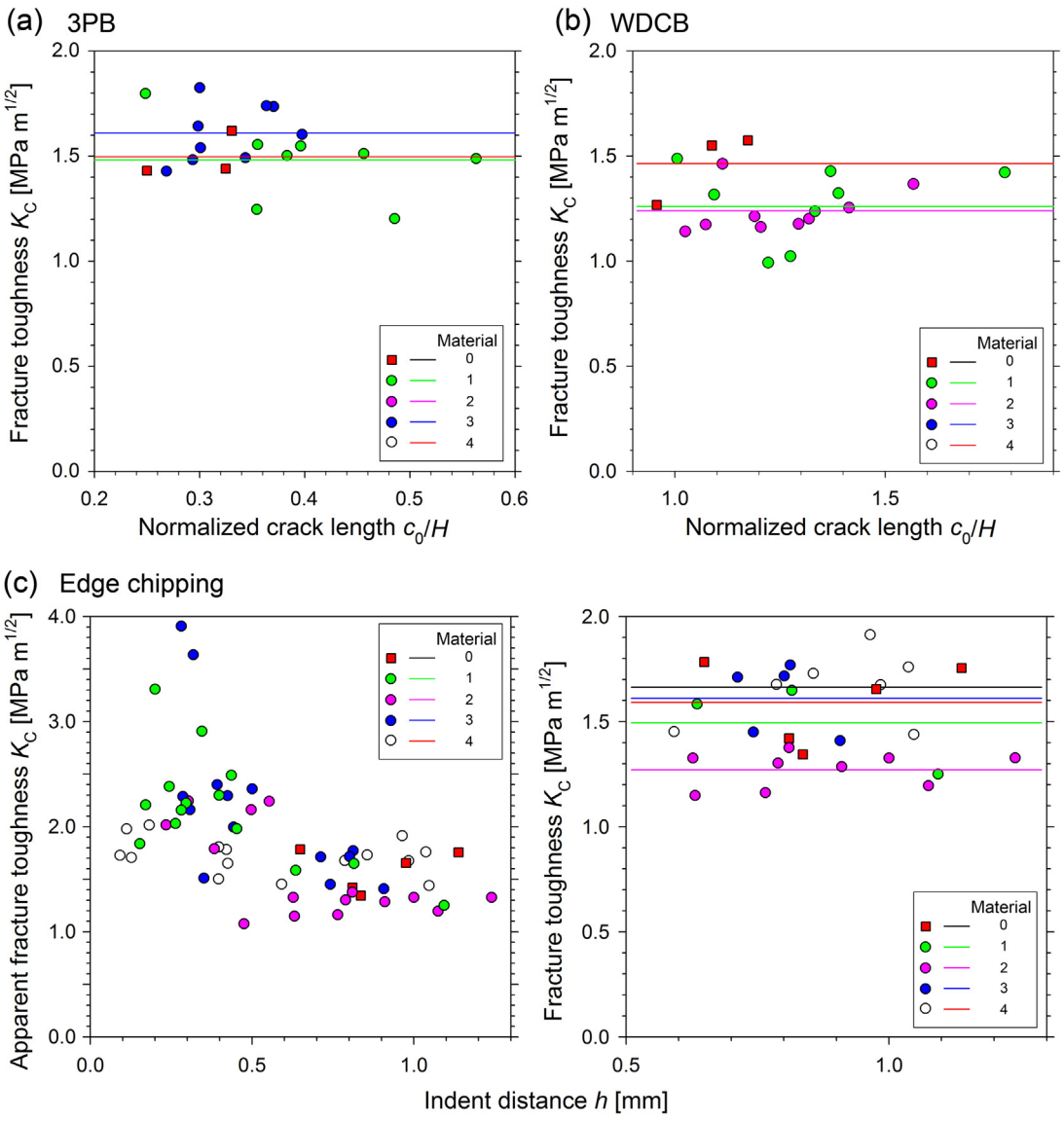

Fig. 6 – Fracture toughness K_C for miniature 3PB (a) WDCB (b) and edge chipping (c) specimens, plotted against relative crack length c_0/H in (a), (b) or indent distance h (c). The material choices are specified in the prints. The validity of K_C in (c) is limited $h > 0.57$, for which the load needed to initiate median cracks under the Vickers tool, P_m, exceed that needed to cause chipping. The valid chipping data are shown in the right-side print of (c). The solid lines in (a) – (c) represent mean values.

Table 2 – Fracture toughness K_C [MPa m$^{1/2}$].*

Material	Control	3PB	WDCB	Edge chipping
0	1.55(0.03)	1.50(0.11)	1.59(0.3)	1.59(0.20)
1	1.32(0.03)	1.48(0.19)	1.26(0.14)	1.49(0.21)
2	1.19(0.05)		1.24(0.11)	1.27(0.08)
3	1.48(0.09)	1.61(0.14)	1.51(0.41)	1.61(0.17)
4	1.52(0.04)		1.57(0.34)	1.66(0.17)

* All are miniature specimens except for the control.

cracks may initiate and grow smoothly under the contact prior to chipping. This can be ascertained by repeat indentation on a sample material prior to the chipping test. For the present dental composites $h > 0.57$ mm suffice, corresponding to $P_m \approx 190$ N. With indent distance on the order of 0.6–0.8 mm, specimen dimensions (B, C) as small as (2.5, 3) mm can be used. These characteristics make the chipping test especially suited for evaluating K_C in graded materials and composites restorations. As an example, we note the significant dependence of DC on tooth size [39]. The 3PB is simple to use but requires introducing a pre-crack. Furthermore, this configuration leads to unstable fracture so that only 1 data point per specimen can

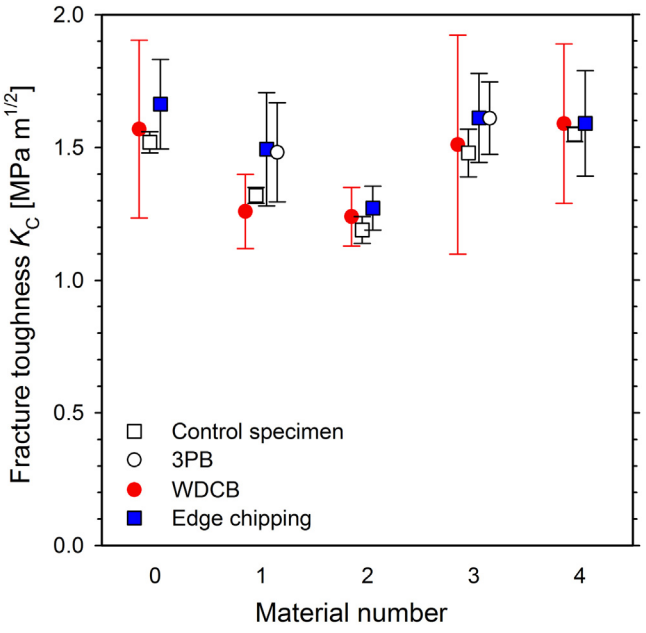

Fig. 7 – Fracture toughness K_C for all materials and specimens used. The open square symbol represents the control specimen.

be obtained. The WDCB specimen requires no loading attachments and furthermore it permits stable cracking for small cracks (c/H <0.3, Fig. 4a). These traits are especially valuable under cyclic loading where, using relatively small crack length, the entire loading spectrum may be studied in a single specimen. For the 3PB and WDCB specimens, the need to introduce a sharp pre-crack (*e.g.*, by a razor blade) was circumvented by defining an inherent flaw size c_F (Eq. (8)). As evident from Figs. 3b and 4b, the function f in Eq. (9) is nearly unity when $c_F/a >$ about 0.5 or, from Eq. (8), $a < 0.51(K_C/\sigma_F)^2$.

5. Conclusions

3PB, wedge and edge chipping cost-effective miniature specimens were developed for determining fracture toughness K_C to within 1–10% error (Fig. 7). The edge chipping test was employed for the first time to evaluate K_C in non-brittle materials. This specimen requires no pre-cracking, which makes it especially useful for evaluating graded materials and *in-situ* studies. The test results indicate that dental resin composites can be chemically altered to reduce post-cure shrinkage without compromising K_C. To insure a valid K_C the width of pre-crack a in the 3PB and WDCB specimens and critical indent distance h_c in the chipping test need be considered in the fracture analysis.

Acknowledgements

This work was sponsored by funding from the Israeli Science Foundation (P.I. H. Chai, ISF Grant no. 810/09) and US National Institute of Dental & Craniofacial Research, National Institutes of Health (P.I. J. Sun, Grant U01DE023752). Financial support was also provided through the ADA Foundation. The authors would like to thank American Dental Association for their supports.

REFERENCES

[1] Fujishima A, Ferracane JL. Comparison of four modes of fracture toughness testing for dental composites. Dent Mater 1996;12:38–43.
[2] Ferracane J, Antonio R, Matsumoto H. Variables affecting the fracture toughness of dental composites. J Dent Res 1987;66:1140–5.
[3] Lin L, Drummond JL. Cyclic loading of notched dental composite specimens. Dent Mater 2010;26:207–14.
[4] Ilie N, Hickel R, Valceanu AS, Huth KC. Fracture toughness of dental restorative materials. Clin Oral Invest 2012;16:489–98.
[5] Ferracane J, Berge H, Condon J. In vitro aging of dental composites in water—effect of degree of conversion, filler volume, and filler/matrix coupling. J Biomed Mater Res 1998;42:465–72.
[6] Ferracane JL. Resin composite-state of the art. Dent Mater 2011;27:29–38.
[7] Ferracane JL. Resin-based composite performance: are there some things we can't predict. Dent Mater 2013;29:51–8.
[8] Beck F, Lettner S, Graf A, Bitriol B, Dumitrescu N, Bauer P, et al. Survival of direct resin restorations in posterior teeth within a 19-year period (1996-2015): a meta-analysis of prospective studies. Dent Mater 2015;31:958–85.
[9] Chai H, Lawn BR. Fracture resistance of molar teeth with mesial-occlusal-distal (MOD) restorations. Dent Mater 2017;33:e283–9.
[10] Gonzalez-Bonet A, Kaufman G, Yang Y, Wong C, Jackson A, Huyang G, et al. Preparation of dental resins resistant to enzymatic and hydrolytic degradation in oral environments. Biomacromolecules 2015;16:3381–8.
[11] Wang X, Huyang G, Palagummi SV, Liu X, Skrtic D, Beauchamp C, et al. High performance dental resin composites with hydrolytically stable monomers. Dent Mater 2018;34:228–37.
[12] Cramer NB, Couch CL, Schreck KM, Carioscia JA, Boulden JE, Stansbury JW, et al. Investigation of thiol-ene and thiol-ene-methacrylate based resins as dental restorative materials. Dent Mater 2010;26:21–8.
[13] Podgorski M, Becka E, Claudino M, Flores A, Shah PK, Stansbury JW, et al. Ester-free thiol-ene dental restoratives-Part A: resin development. Dent Mater 2015;31:1255–62.
[14] Bacchi A, Pfeifer CS. Rheological and mechanical properties and interfacial stress development of composite cements modified with thio-urethane oligomers. Dent Mater 2016;32:978–86.
[15] Huyang G, Debertin AE, Sun J. Design and development of self-healing dental composites. Mater Des 2016;94:295–302.
[16] Wu JL, Weir MD, Zhang Q, Zhou CJ, Melo MAS, Xu HHK. Novel self-healing dental resin with microcapsules of polymerizable triethylene glycol dimethacrylate and N,N-dihydroxyethyl-p-toluidine. Dent Mater 2016;32:294–304.
[17] Huyang G, Sun JR. Clinically applicable self-healing dental resin composites. MRS Adv 2016;1:547–52.
[18] Yang Y, Reipa V, Liu G, Meng Y, Wang X, Mineart KP, et al. pH-Sensitive compounds for selective inhibition of acid-producing bacteria. ACS Appl Mater Interfaces 2018;10:8566–73.
[19] Hwang G, Koltisko B, Jin XM, Koo H. Nonleachable imidazolium-incorporated composite for disruption of

bacterial clustering, exopolysaccharide-matrix assembly, and enhanced biofilm removal. ACS Appl Mater Interfaces 2017;9:38270–80.
[20] Antonucci JM, Zeiger DN, Tang K, Lin-Gibson S, Fowler BO, Lin NJ. Synthesis and characterization of dimethacrylates containing quaternary ammonium functionalities for dental applications. Dent Mater 2012;28:219–28.
[21] Cheng L, Weir MD, Xu HHK, Antonucci JM, Kraigsley AM, Lin NJ, et al. Antibacterial amorphous calcium phosphate nanocomposites with a quaternary ammonium dimethacrylate and silver nanoparticles. Dent Mater 2012;28:573–83.
[22] Sun J, Eidelman N, Lin-Gibson S. 3D mapping of polymerization shrinkage using X-ray micro-computed tomography to predict microleakage. Dent Mater 2009;25:314–20.
[23] Sun JR, Fang R, Lin N, Eidelman N, Lin-Gibson S. Nondestructive quantification of leakage at the tooth-composite interface and its correlation with material performance parameters. Biomaterials 2009;30: 4457–62.
[24] Chai H, Kaizer M, Chughtai A, Tong H, Tanaka C, Zhang Y. On the interfacial fracture resistance of resin-bonded zirconia and glass-infiltrated graded zirconia. Dent Mater 2015;31:1304–11.
[25] McCormick NJ. Edge flaking of brittle materials. Adv Eng Ceram Lond, December, 1989, 1990:307–18.
[26] Quinn JB, Quinn GD. Material properties and fractography of an indirect dental resin composite. Dent Mater 2010;26:589–99.
[27] Gogotsi G, Galenko V, Mudrik S, Ozersky B, Khvorostyany V, Khristevich T. Fracture resistance estimation of elastic ceramics in edge flaking: EF baseline. J Eur Ceram Soc 2010;30:1223–8.
[28] Chai H, Lawn BR. A universal relation for edge chipping from sharp contacts in brittle materials: a simple means of toughness evaluation. Acta Mater 2007;55:2555–61.
[29] Petit F, Vandeneede V, Cambier F. Ceramic toughness assessment through edge chipping measurements—influence of interfacial friction. J Eur Ceram Soc 2009;29:2135–41.
[30] Mohajerani A, Spelt J. Edge chipping of borosilicate glass by blunt indentation. Mech Mater 2010;42:1064–80.
[31] Chai H. On the mechanics of edge chipping from spherical indentation. Int J Fract 2011;169:85–95.
[32] Hervas I, Montagne A, Van Gorp A, Bentoumi M, Thuault A, Iost A. Fracture toughness of glasses and hydroxyapatite: a comparative study of 7 methods by using Vickers indenter. Ceram Int 2016;42:12740–50.
[33] Engineer's Handbook. Reference Table — Coefficient of friction.
[34] Bower AF. Applied mechanics of solids. CRC press; 2009.
[35] Srawley JE, Brown WF. Fracture toughness testing methods. Fracture toughness testing and its applications. ASTM International; 1965.
[36] Chai H, Ravichandran G. Transverse fracture in multilayers from tension and line-wedge indentation. Int J Fract 2007;145:299–312.
[37] Lawn B. Fracture of brittle solids. Cambridge University Press; 1993.
[38] Sun J, Eidelman N, Lin-Gibson S. 3D mapping of polymerization shrinkage using X-ray micro-computed tomography to predict microleakage. Dent Mater 2009;25:314–20.
[39] Alexander Tarimo S, Mabula Machibya F, Zhi Min Z. Influence of tooth thickness on degree of conversion of photo-activated resin composite irradiated through the tooth. Int J Dent Oral Sci 2017;4:450–6.